iTRVZ: liquid nano-platform for signal integration on the plasma membrane

Taka A. Tsunoyama[1], Christian Hoffmann[2], Bo Tang[1], Koichiro M. Hirosawa[3], Yuri L. Nemoto[1], Rinshi S. Kasai[3], Takahiro K. Fujiwara[4], Kenich G.N. Suzuki[3,4], Dragomir Milovanovic[2], Akihiro Kusumi[1,4]*

[1]Membrane Cooperativity Unit, Okinawa Institute of Science and Technology Graduate University (OIST), Onna-son, Okinawa 904-0495, Japan. [2]Laboratory of Molecular Neuroscience, German Centre for Neurodegenerative Diseases (DZNE) 10117 Berlin, Germany. [3]Institute for Glyco-Core Research (iGCORE), Gifu University, Gifu 501-1193, Japan. [4]Institute for Integrated Cell-Material Sciences (WPI-iCeMS), Kyoto University, Kyoto 606-8501, Japan.

*To whom correspondence should be addressed:
Akihiro Kusumi
e-mail: akihiro.kusumi@oist.jp
ORCID: 0000-0002-9558-6950
Ph: 011-81-98-982-3568, Fx: 011-81-98-966-1062

Summary

Signalling is one of the most important functions of the cellular plasma membrane (PM). A variety of extracellular signalling molecules bind to their specific receptors in the PM, and the engaged receptors in turn trigger various cytoplasmic signalling cascades. These signalling pathways are intertwined and affect each other, in a process called crosstalk, which enables the cells to fine tune the overall signal. The crosstalk of different receptor signalling pathways has been examined quite extensively, but the platform responsible for signal integration has never been discovered. Here, using single-molecule imaging, we found a nanometer-scale (50-80 nm) liquid-like protein assembly on the PM cytoplasmic surface (at a density of ~2-μm apart from each other on average, with a lifetime of ~10 s), working as the signal transduction and integration platform for receptors, including GPI-anchored receptors (GPI-ARs), receptor-type tyrosine kinases (RTKs), and GPCRs. The platform consists of integrin, talin, RIAM, VASP, and zyxin, and is thus termed iTRVZ. These molecules are known as focal-adhesion constituents, but iTRVZ is distinct from focal adhesions, because iTRVZ exists on both the apical and basal PMs and lack vinculin. The iTRVZ formation is driven by specific protein-protein interactions, liquid-liquid phase separation, and interactions with actin filaments and raft domains via PI(4,5)P_2. iTRVZ integrates and amplifies the GPI-AR and RTK signals in a strongly non-linear fashion, and thus works as an AND gate and noise filter. These findings greatly advance our understanding of the mechanism for crosstalk between signalling pathways.

Main text

Signalling pathways downstream from receptors are the targets of extensive investigations. In particular, understanding how each signalling pathway is integrated into coordinated cellular signal responses is one of the most critical issues in today's signalling research[1]. We hypothesised that PM-associated structures that function as platforms for signal integration might exist. Since integrins are involved in the signalling of receptor-type tyrosine kinases (RTKs)[2], immunoglobulin E Fc receptor[3], and glycosylphosphatidylinositol (GPI)-anchored receptors (GPI-ARs), including CD59, Thy1, and CD55[4–9], we examined the possibility that an integrin-centered signal integration platform might exist on the PM cytoplasmic surface.

Talin clusters recruit receptors

Talin, a focal-adhesion (FA) protein, binds to integrins and various signalling molecules[10,11]. We examined the possibility that talin might play a central role in the formation and function of the hypothetical signal integration platform. We expressed tagged-talin1 molecules (four different tags) in talin1/2 double-knockout mouse embryonic fibroblasts (dKO MEFs)[11], at levels comparable to that of endogenous talin1 (**Extended Data Fig. 1a-k**). Our advanced single-molecule imaging revealed that fluorescently-labeled talin1 (talin; in the following, talin1 is described as talin) formed numerous clusters on the cytoplasmic surface of the *apical* PM, where virtually no FAs exist[12], even without stimulation (**Extended Data Fig. 1i, Supplementary Video 1**).

Clustered CD59, containing an average of five CD59 molecules simulating the ligated signalling-active CD59[4,5], and ligated PDGFR were transiently and repeatedly recruited to the talin clusters on the apical PM, with a dwell lifetime of each recruitment lasting for ~0.3 s (exponential decay time constant, τ_2; **Fig. 1a, b, Supplementary Videos 2, 3**; **Materials and methods**). The recruitments of these receptors suggested that the talin clusters might function as the signalling platform for both receptors.

Liquid-like talin-zyxin nanoclusters

We found that zyxin, another FA protein, also forms clusters on the *apical* PM in zyxin-KO MEF cells[13] rescued with tagged zyxin proteins expressed at levels similar to that of endogenous zyxin (**Extended Data Fig. 1e-i, Supplementary Video 1**). Each talin and zyxin cluster contains a median of 4.0 and 4.8 copies of talin and zyxin, respectively (with broad distributions between 2 and 15 copies/cluster) (**Fig. 1c**). These clusters exist on the apical PM densely, with a mean number

density of ~0.25 clusters/μm^2 for both talin and zyxin (**Fig. 1d**). This number density is comparable to that of clathrin-coated structures[14].

Approximately 70% of the talin and zyxin clusters were colocalised with each other (**Fig. 1e** and **Data Fig. 1j, k**, respectively), suggesting that these clusters are co-clusters of talin and zyxin. Meanwhile, this 70% colocalisation of talin and zyxin clusters indicated that some of them might contain 0-2 copies of the talin and zyxin/cluster (the presence of 1~2 copies in the cluster could be missed under the employed imaging conditions). We refer to these altogether as "talin-zyxin clusters". Partial actin depolymerisation with latrunculin A and cytochalasin D, and myosin deactivation with the ROCK inhibitor Y27632 reduced both the number density of talin clusters in the apical PM and the number of talin molecules within a talin cluster, suggesting that the formation of the talin-zyxin clusters requires the intact actin-myosin system. Meanwhile, stimulation by CD59 clustering or PDGF addition did not induce any changes in either the talin cluster number density or the talin number within a cluster (**Fig. 1c, d**).

The lifetime of the talin-zyxin clusters themselves exhibited the presence of two components (**Fig. 1f**): ~15% lasted for ~1 s and ~85% lasted for ~10 s (addition averages of talin and zyxin). These lifetimes would represent both the dissociation of the clusters from the apical PM and the disintegration of the clusters. Meanwhile, the lifetime of talin clusters without zyxin observed in the zyxin-KO MEFs and the lifetime of zyxin clusters without talin in talin-dKO MEFs were both 1.1 s, and after rescue, the lifetimes became 9.5 s and 7.7 s, respectively (**Extended Data Fig. 1l**; all SEM values given in figures). These results indicate that the ~1-s component (~15%) of the talin-zyxin clusters represents those that do not contain either talin or zyxin. The value of 85% for the 7.7~9.5-s component is indeed close to the 70% estimated for the clusters containing both (more than two) talin and zyxin proteins.

Single molecules of talin and zyxin repeatedly entered and exited from the clusters, with dwell lifetimes in the talin-zyxin cluster of 2.1 and 1.4 s, respectively (**Fig. 1g, Extended Data Fig. 1m**), indicating that these molecules exchange with those in the bulk cytoplasm several times during the lifetime of the talin-zyxin cluster. This result indicates the liquid-like characteristics of the clusters.

Photoactivation localisation microscopy (PALM) of talin and zyxin in fixed cells, followed by a Voronoï tessellation analysis[15,16], detected their nanoscale clusters (median diameter = 60 nm) on the *apical* PM at a number density of 0.35 clusters/μm^2 (mean; the average for talin and zyxin) (**Fig. 1h-k, Extended Data Fig. 2a-g**), consisting of a mean of 6.1 and 8.2 copies of talin and zyxin, respectively (slightly overestimated because clusters containing fewer than 3 copies were undetectable; **Fig. 1j**).

In summary, talin-zyxin clusters are liquid-like, nanoscale clusters with a lifetime on the PM of ~10 s, where constituent molecules and engaged receptors (PDGFR and CD59) are exchanging on the time scale of 0.3 - 2.1 s (see the intensity fluctuations of the cluster in **Supplementary Video 4**). Talin-zyxin clusters were found in all five cell lines examined here (**Extended Data Fig. 3a**), suggesting that these clusters broadly exist in mammalian cells.

iTRVZ contains FA proteins

To facilitate the observations of single-molecule recruitment to the talin-zyxin clusters in the *apical PM*, we generated a human T24 epithelial cell line stably expressing SNAPf-talin (called T24-T; together with endogenous talin1, expressing 1.7x more talin than that in wild-type cells). The apical PM of the T24 cell is quite flat, facilitating single-molecule imaging (**Extended Data Fig. 3b-e**). As in MEFs, the engaged CD59 and PDGFR were transiently recruited to the talin-zyxin clusters in T24-T cells (**Extended Data Fig. 3f-i**).

We next investigated the presence of other FA proteins in the talin-zyxin clusters (**Extended Data Fig. 3j**). To systematically evaluate the propensity of the FA proteins to colocalise with the talin-zyxin clusters at the level of single molecules, we employed the "colocalisation index", which is a measure of finding a molecule within a 50 nm radius circle around the center of the talin cluster relative to far distances[17] (as a control, all fluorescent spots were shifted by 1 μm with random angles in 2D) (**Extended Data Fig. 3k, Methods**). β3 integrin (i), RIAM (R), VASP (V), and zyxin (Z) were remarkably colocalised with the talin (T) clusters even before PDGF stimulation, and therefore, we coined the name iTRVZ for the talin-zyxin cluster. Meanwhile, paxillin, vinculin, and N-WASP were not colocalised, showing that although iTRVZ contains FA proteins, its protein composition is distinct from that of the mature FA[18] (**Fig. 2a**). The actin-binding proteins α-actinin and filamin were also colocalised with iTRVZ. Upon PDGF stimulation, interestingly, the colocalisations of the T, R, V, and Z proteins were not increased, whereas those of integrin and FAK were increased (**Fig. 2a**). Consistently, the dwell lifetime of FAK at the iTRVZ was elongated (**Extended Data Fig. 3l, m, Supplementary Video 5**). Furthermore, paxillin and N-WASP were recruited to iTRVZ after stimulation.

iTRVZ is involved in many signalling pathways

The PDGF stimulation induced the iTRVZ recruitment of FAK, PLCγ1, Lyn, PI3K, and Akt (**Fig. 2a, b**). Furthermore, PLCγ1 was transiently recruited to iTRVZ upon the engagements of GPI-ARs (CD59 and Thy1) and RTKs (PDGFR and EGFR), and PLCβ was recruited upon the stimulation of a GPCR (UTP receptor, P2Y) (**Fig. 2c, d**). The recruitment of these molecules was reduced by the inhibitors for FAK and SFK (**Fig. 2c**). The PDGF-induced PLCγ1 recruitment additionally occurred

on the PM outside the iTRVZ (**Extended Data Fig. 3n, o**), indicating that the PDGFR's downstream signal occurs both inside and outside the iTRVZ. However, the PLCγ1's recruitment per unit area is ~30 times greater in the iTRVZ than in the region outside the PM (**Fig. 2e**, see also **Extended Data Fig. 3n, o**), indicating that the signalling reactions would occur much more efficiently in iTRVZ (**Fig. 2f**). As such, iTRVZ works as a platform for various signalling pathways.

iTRVZ is bound by PI(4,5)P_2 and raft lipids

The involvement of phosphoinositides in iTRVZ was examined because PLCγ1 is recruited to iTRVZ, and talin and RIAM bind PI(4,5)P_2[19,20] (**Fig. 3a-c, Supplementary Video 6**). Using probes for various phosphoinositides[21], PI(4)P and PI(4,5)P_2, but not PI(3)P and PI(3,4)P_2, were localised at the iTRVZ both before and after PDGF stimulation equally, but PI(3,4,5)P_3 was found only after stimulation (**Fig. 3c**). PI3K, which generates PI(3,4,5)P_3 from PI(4,5)P_2, was recruited to the iTRVZ only after PDGF stimulation (**Fig. 2b**), whereas PIP5K, which generates PI(4,5)P_2 and binds to talin[19] and MARCKS, a PI(4,5)P_2-sequestering protein, were recruited even before stimulation without any changes after stimulation. These results suggest that PI(3,4,5)P_3 is generated from PI(4,5)P_2 by the PI3K recruited to iTRVZ upon stimulation.

Meanwhile, typical raftophilic lipids, cholesterol and sphingomyelin (SM), were colocalised with the iTRVZ[22,23] (**Fig. 3b, c**). The number density and size (talin number) of the iTRVZ were reduced after partial depletions of cholesterol and PI(4,5)P_2[4,5,24,25] (**Extended Data Fig. 4a-k**). Phosphatidylserine (PS), with its long, saturated acyl chain subfraction putatively involved in the aster formation of GPI-ARs and actin filaments[9,26,27], was also colocalised with the iTRVZ (**Fig. 3c**). These results suggest that iTRVZ is supported by raft-lipid interactions[28] by way of PI(4,5)P_2 (and possibly long, saturated-chain PS). Meanwhile, the RTK's downstream signalling molecules JAK1, K-Ras, and Raf were not recruited to the iTRVZ (**Fig. 3d**).

In conclusion, iTRVZ, formed with the aid of raft domains by way of PI(4,5)P_2 and PS, recruits various signalling molecules downstream from the activated receptors, and works as the signal transduction platform for GPI-ARs, RTKs, and GPCRs (**Fig. 3e**). Namely, iTRVZ is shared by these receptor signalling pathways, suggesting the possibility that signal crosstalk and integration are induced there.

iTRVZ as a cooperative signal integrator

Indeed, iTRVZ cooperatively and non-linearly integrates the PDGFR (RTK) and CD59 (GPI-AR) signals. First, we weakly stimulated the cells by adding either 20 pM PDGF (physiological concentration in the serum[29]) or 20 nM anti-CD59 mAb coated beads for CD59 clustering, which are 1/1,000 and 1/100 concentrations of our standard conditions, respectively. They induced much

lower PLCγ1 recruitment to the iTRVZ and Ca^{2+} responses than those in our standard conditions (**Fig. 4a, b; Extended Data Fig. 5a**). When we added both stimulants at the same time, the PLCγ1 recruitment to iTRVZ and the Ca^{2+} responses became greater than the sum of those induced by separate stimulations, by factors of 4.7 and 6.8, respectively (**Fig. 4a, b, Extended Data Fig. 5a**), clearly demonstrating the cooperative, non-linear integration of the two signals.

This non-linear integrated amplification depended on iTRVZ, because it did not happen with zyxin-KO cells. However, it was recovered by the addition of the intrinsically disordered region [IDR] of zyxin, which is responsible for the formation of zyxin-talin co-clusters (**Fig. 4a, b; Extended Data Fig. 5b, c;** for the zyxin's IDR, see the next subsection).

The non-linear integration depended on the activation of both FAK and SFK at iTRVZ (**Fig. 4a, b; Extended Data Fig. 5c**), and did not occur outside the iTRVZ (**Fig. 4b**). Since the weak CD59 stimulation induced the FAK recruitment to iTRVZ more effectively than the SFK recruitment, and the weak PDGF stimulation triggered SFK recruitment but not the FAK recruitment (**Extended Data Fig. 5d**), the cooperative integration is considered to be induced by the simultaneous recruitment of SFK and FAK to iTRVZ, causing their upward spiral activations (**Fig. 4c; Extended Data Fig. 5e**). In conclusion, iTRVZ works as a cooperative signal integrator for multiple, coincidental signals due to the co-activation of SFK and FAK in the fluid nano-region.

Nanoscale LLPS for iTRVZ formation

The iTRVZ's main constituent molecules, RIAM, VASP, and zyxin, contain long intrinsically disordered regions (IDRs)[30] (**Fig. 4d, Extended Data Fig. 6a, b**), which are often involved in liquid-liquid phase separation (LLPS)[31–34]. Therefore, we examined the involvement of LLPS in iTRVZ formation.

First, iTRVZ was reduced in size (the talin number) in MEF cells after a 1,6-hexanediol treatment, which is known to disperse liquid condensates (**Fig. 1c**). Second, purified zyxin and VASP formed liquid-like co-condensates *in vitro* at endogenous concentrations of 0.7~3.0 and 0.25 ~0.7 μM, respectively (**Fig. 4e, f, Extended Data Fig. 7a-j**). In T24 cells, micron-scale condensates of zyxin and VASP were never observed at endogenous expression levels, but were formed (always co-clustered) in cells overexpressing the proteins at ~14 μM average concentrations in the cytoplasm (**Fig. 4g, h, Extended Data Fig. 7k-m, Supplementary Video 7**), probably due to the presence of higher concentrations of proteins and other electrolytes like ATP[35]. The results obtained using WT and mutant zyxin (**Fig. 4d**), as well as those of VASP and RIAM, showed that the non-phosphorylated IDR domains are essential for their recruitment to iTRVZ (**Fig. 4i; Extended Data Fig. 8a, b**).

To further examine the IDR involvement in iTRVZ formation and signal transduction, we produced seven zyxin-KO MEF cell lines expressing different zyxin mutants (**Extended Data Fig. 9a-f**). By comparing the sizes (talin numbers) and lifetimes of the iTRVZ in these cell lines (**Extended Data Fig. 9d, e**), we found that the three LIM domains near the N-terminus, the IDR (including the Pro-rich domain), and the dephosphorylation of zyxin enhance iTRVZ formation. Upon PDGF stimulation, the four cell lines expressing zyxin lacking these domains or expressing phosphomimetic zyxin exhibited lower Ca^{2+} responses and Akt phosphorylation, as compared with the zyxin-KO MEF cells rescued with the full-length zyxin (**Fig. 4j-l, Extended Data Fig. 9g, h**). As described in the previous subsection, the non-linear integration of the weak CD59 and PDGF signals did not occur in cells without zyxin expression, but was recovered by expressing zyxin's IDR (**Fig. 4b, Extended Data Fig. 5a**). In conclusion, these data demonstrate that the IDR-based interactions are critical for generating the functional iTRVZ platform.

Discussion

We identified a nanoscale liquid-like signal integration platform on the PM, iTRVZ (**Extended Data Fig. 10**), which exists in both the apical and basal PMs. The iTRVZ platform is commonly used for the signalling pathways of three representative receptor classes: GPI-AR (CD59, Thy1), RTK (PDGFR, EGFR), and GPCR (UTP receptor, P2Y) (**Fig. 2c**). The recruited receptors and downstream signalling molecules can interact at iTRVZ extremely rapidly and efficiently, due to the very small sizes of the iTRVZ platform (50 ~ 80 nm in diameter) and its liquid nature.

iTRVZ works as a cooperative and non-linear integrator and coincidence detector/amplifier of the signals from these different signalling pathways. Non-linear integration and coincidence detection/amplification would be critically important for inducing strong downstream signals when two separate external signals are received by the cell at about the same time, as well as for filtering out the accidentally evoked noise that would be prevalent in the cytoplasm[36,37].

The lifetime of iTRVZ is ~10 s, and its constituent molecules and recruited receptors and signalling molecules exchange with those in the bulk cytoplasm in the time scale of 0.2 - 3 s (**Fig. 1f, Extended Data Fig. 1l**), although the overall receptor signal in a whole cell tends to last for several minutes or longer. This indicates that each iTRVZ platform would create unit pulse-like signals on the order of seconds, and that the signal observed for a whole single cell, like the phosphorylation levels and Ca^{2+} mobilisation, would be the result of the summation of the unit pulse-like signals from many iTRVZ[4,5,38,39]. In addition, the limited iTRVZ lifetime and dwell lifetimes of signalling molecules would be useful for turning off the signals quickly and reliably: the output signal from each iTRVZ would be stopped within ~10 s without fail because iTRVZ will

self-destruct and/or self-dissociate from the PM in 10 s. Similar transient liquid-like nanoscale signalling platforms might exist for other signalling systems[34,40] including those in immune cells[3,40].

The iTRVZ formation and signalling are aided by LLPS due to the IDR-IDR interactions of zyxin and VASP, and perhaps those of RIAM and other constituent molecules, as well as by the raft domains by way of PI(4,5)P_2 and possibly the long, saturated acyl chain of PS. The occurrence of LLPS on the nanometer scale has been suggested recently[41]. The liquid-like loose assemblies of iTRVZ, supported by the IDR-based LLPS, probably make iTRVZ quite versatile, to allow for the recruitment of a variety of receptors and signalling molecules, the enhancement of their interactions, their rapid departures from iTRVZ, and its self-destruction in 10 s. In the basal PM, some of the iTRVZs might convert into nano-scale nascent FAs upon the applied stress via integrin and vinculin recruitment[10,18,42]. iTRVZ was found in all of the cell lines examined in this study, and thus we conclude that it is a fundamentally important signal integration platform ubiquitously functioning in mammalian cells.

Main references

1. Taniguchi, C. M., Emanuelli, B. & Kahn, C. R. Critical nodes in signalling pathways: insights into insulin action. *Nat. Rev. Mol. Cell Biol.* **7**, 85–96 (2006).

2. Chen, Z. *et al.* EGFR family and Src family kinase interactions: mechanics matters? *Curr. Opin. Cell Biol.* **51**, 97–102 (2018).

3. Wakefield, D. L., Holowka, D. & Baird, B. The FcεRI signaling cascade and integrin trafficking converge at patterned ligand surfaces. *Mol. Biol. Cell* **28**, 3383–3396 (2017).

4. Suzuki, K. G. N., Fujiwara, T. K., Edidin, M. & Kusumi, A. Dynamic recruitment of phospholipase Cγ at transiently immobilized GPI-anchored receptor clusters induces IP_3–Ca^{2+} signaling: single-molecule tracking study 2. *J. Cell Biol.* **177**, 731–742 (2007).

5. Suzuki, K. G. N. *et al.* GPI-anchored receptor clusters transiently recruit Lyn and Gα for temporary cluster immobilization and Lyn activation: single-molecule tracking study 1. *J. Cell Biol.* **177**, 717–730 (2007).

6. Cui, X. *et al.* Shear stress-mediated changes in the expression of complement regulatory protein CD59 on human endothelial progenitor cells by ECM-integrinαVβ3-F-actin pathway in vitro. *Biochem. Biophys. Res. Commun.* **494**, 416–421 (2017).

7. Morris, R. J. Thy-1, a pathfinder protein for the post-genomic era. *Front. Cell Dev. Biol.* **6**, 173 (2018).

8. Strainic, M. G. *et al.* CD55 is essential for $CD103^+$ dendritic cell tolerogenic responses that protect against autoimmunity. *Am. J. Pathol.* **189**, 1386–1401 (2019).

9. Kalappurakkal, J. M. *et al.* Integrin mechano-chemical signaling generates plasma membrane nanodomains that promote cell spreading. *Cell* **177**, 1738-1756. e23 (2019).

10. Kanchanawong, P. *et al.* Nanoscale architecture of integrin-based cell adhesions. *Nature* **468**, 580–584 (2010).

11. Theodosiou, M. *et al.* Kindlin-2 cooperates with talin to activate integrins and induces cell spreading by directly binding paxillin. *eLife* **5**, e10130 (2016).

12. Yamada, K. M. & Sixt, M. Mechanisms of 3D cell migration. *Nat. Rev. Mol. Cell Biol.* **20**, 738–752 (2019).

13. Hoffman, L. M. *et al.* Genetic ablation of zyxin causes Mena/VASP mislocalization, increased motility, and deficits in actin remodeling. *J. Cell Biol.* **172**, 771–782 (2006).

14. Fujiwara, T. K. *et al.* Confined diffusion of transmembrane proteins and lipids induced by the same actin meshwork lining the plasma membrane. *Mol. Biol. Cell* **27**, 1101–1119 (2016).

15. Sengupta, P., Van Engelenburg, S. & Lippincott-Schwartz, J. Visualizing cell structure and function with point-localization superresolution imaging. *Dev. Cell* **23**, 1092–1102 (2012).

16. Levet, F. *et al.* SR-Tesseler: a method to segment and quantify localization-based super-resolution microscopy data. *Nat. Methods* **12**, 1065–1071 (2015).

17. Stone, M. B. & Veatch, S. L. Steady-state cross-correlations for live two-colour super-resolution localization data sets. *Nat. Commun.* **6**, 7347 (2014).

18. Han, S. J. *et al.* Pre-complexation of talin and vinculin without tension is required for efficient nascent adhesion maturation. *eLife* **10**, e66151 (2021).

19. Paolo, G. D. *et al.* Recruitment and regulation of phosphatidylinositol phosphate kinase type 1γ by the FERM domain of talin. *Nature* **420**, 85–89 (2002).

20. Cho, EA. *et al.* Phosphorylation of RIAM by src promotes integrin activation by unmasking the PH domain of RIAM. *Structure* **29**, 320-329. e4 (2021).

21. Furutani, M., Tsujita, K., Itoh, T., Ijuin, T. & Takenawa, T. Application of phosphoinositide-binding domains for the detection and quantification of specific phosphoinositides. *Anal. Biochem.* **355**, 8–18 (2006).

22. Maekawa, M. Domain 4 (D4) of perfringolysin O to visualize cholesterol in cellular membranes—the update. *Sensors* **17**, 504 (2017).

23. Endapally, S. *et al.* Molecular discrimination between two conformations of sphingomyelin in plasma membranes. *Cell* **176**, 1040-1053. e17 (2019).

24. Idevall-Hagren, O., Dickson, E. J., Hille, B., Toomre, D. K. & De Camilli, P. Optogenetic control of phosphoinositide metabolism. *Proc. Natl. Acad. Sci. USA* **109**, E2316–E2323 (2012).

25. Santos, M. de S., Naal, R. M. Z. G., Baird, B. & Holowka, D. Inhibitors of PI(4,5)P_2 synthesis reveal dynamic regulation of IgE receptor signaling by phosphoinositides in RBL mast cells. *Mol. Pharmacol.* **83**, 793–804 (2013).

26. Gowrishankar, K. *et al.* Active remodeling of cortical actin regulates spatiotemporal organization of cell surface molecules. *Cell* **149**, 1353–1367 (2012).

27. Lee, S. *et al.* Transport through recycling endosomes requires EHD1 recruitment by a phosphatidylserine translocase. *EMBO J.* **34**, 669–688 (2015).

28. Simons, K. & Sampaio, J. L. Membrane organization and lipid rafts. *Cold Spring Harb. Perspect. Biol.* **3**, a004697 (2011).

29. Rossi, E. *et al.* Increased plasma levels of platelet-derived growth factor (PDGF-BB + PDGF-AB) in patients with never-treated mild essential hypertension. *Am. J. Hypertens.* **11**, 1239–1243 (1998).

30. Piovesan, D. *et al.* MobiDB: intrinsically disordered proteins in 2021. *Nucleic Acids Res.* **49**, D361–D367 (2020).

31. Milovanovic, D., Wu, Y., Bian, X. & De Camilli, P. A liquid phase of synapsin and lipid vesicles. *Science* **361**, eaat5671 (2018).

32. Feng, Z., Chen, X., Wu, X. & Zhang, M. Formation of biological condensates via phase separation: Characteristics, analytical methods, and physiological implications. *J. Biol. Chem.* **294**, 14823–14835 (2019).

33. Case, L. B., Ditlev, J. A. & Rosen, M. K. Regulation of transmembrane signaling by phase separation. *Annu. Rev. Biophys.* **48**, 1–30 (2019).

34. Jaqaman, K. & Ditlev, J. A. Biomolecular condensates in membrane receptor signaling. *Curr. Opin. Cell Biol.* **69**, 48–54 (2021).

35. Hoffmann, C. *et al.* Synapsin condensates recruit alpha-synuclein. *J. Mol. Biol.* **433**, 166961 (2021).

36. Huang, W. Y. C. *et al.* A molecular assembly phase transition and kinetic proofreading modulate Ras activation by SOS. *Science* **363**, 1098–1103 (2019).

37. Klosin, A. *et al.* Phase separation provides a mechanism to reduce noise in cells. *Science* **367**, 464–468 (2020).

38. Suzuki, K. G. N. *et al.* Transient GPI-anchored protein homodimers are units for raft organization and function. *Nat. Chem. Biol.* **8**, 774–783 (2012).

39. Kusumi, A., Tsunoyama, T. A., Hirosawa, K. M., Kasai, R. S. & Fujiwara, T. K. Tracking single molecules at work in living cells. *Nat. Chem. Biol.* **10**, 524–532 (2014).

40. Su, X. *et al.* Phase separation of signaling molecules promotes T cell receptor signal transduction. *Science* **352**, 595–599 (2016).

41. Peng, S. *et al.* Phase separation at the nanoscale quantified by dcFCCS. *Proc. Natl Acad. Sci. USA* **117**, 27124–27131 (2020).

42. Massou, S. *et al.* Cell stretching is amplified by active actin remodelling to deform and recruit proteins in mechanosensitive structures. *Nat. Cell Biol.* **22**, 1011–1023 (2020).

Main figures

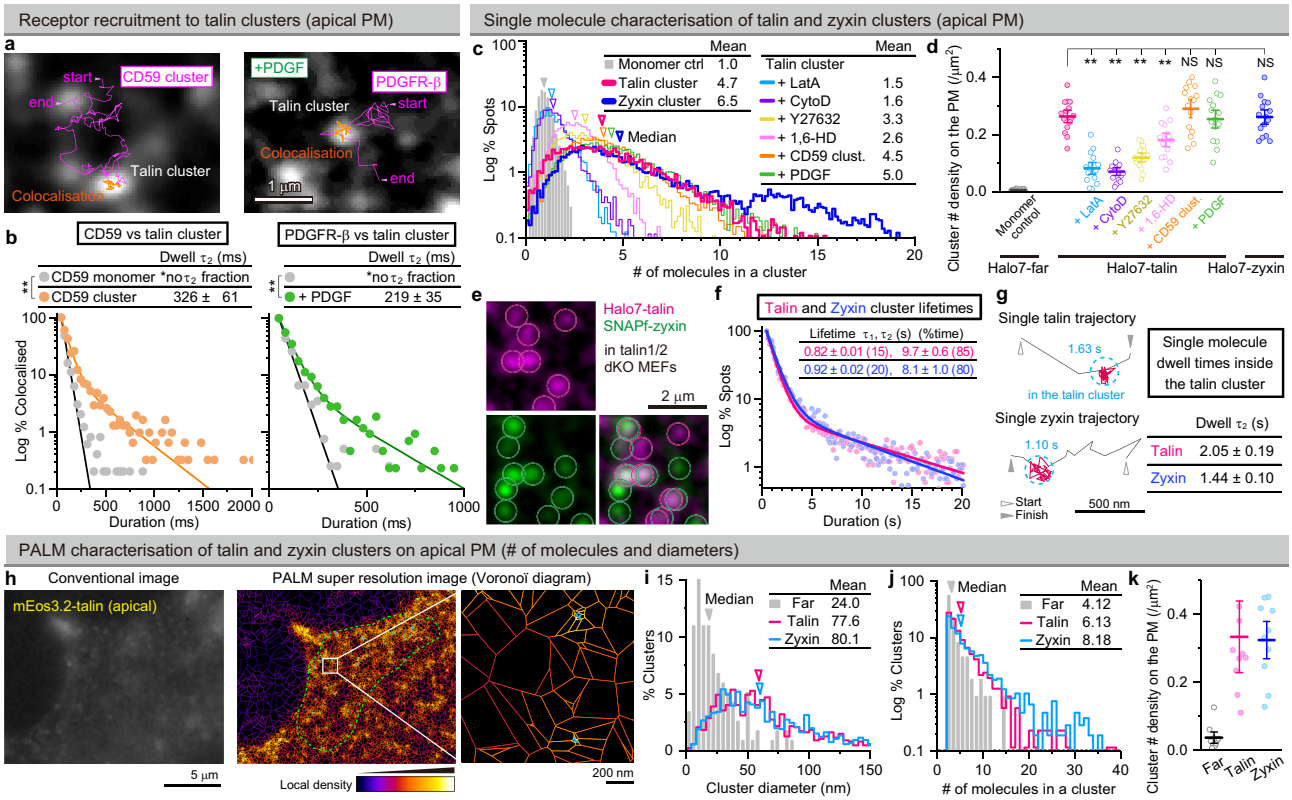

Figure 1 | Co-clusters of talin and zyxin with ~10-s lifetimes on the apical PM recruit receptors.

a, b, Engaged CD59 and PDGFR (trajectories) were recruited to talin clusters (white spots in **a**) with dwell lifetimes of 0.33 and 0.22 s, respectively (**b**) (**Supplementary Videos 2, 3**). Throughout this work, we found that the dwell time distributions could be fitted by double exponential functions, and the longer decay time constants, τ_2s, provided biologically meaningful lifetimes (**the main text; Methods**), while the fitting error provided the SEM. Statistical details including the employed test and *P* values are summarised in the **Source Data**. In figures, **, *, and NS indicate $P<0.01$, $0.01\leq P<0.05$, and $P\geq 0.05$, respectively.

c, Distributions of the numbers of molecules residing in each cluster (monomer control: farnesylated Halo7 [Halo7-far]).

d, Number densities of talin and zyxin clusters on the apical PM (dots for individual cells; bars for mean ± SEM).

e, Typical dual color images of talin and zyxin clusters (indicated by circles); ~70% clusters are colocalised with each other (**Extended Data Fig. 1j, k**).

f, Lifetime distributions of individual clusters.

g, Typical trajectories of single talin and zyxin molecules, exhibiting their temporary recruitment

(magenta trajectories) to talin clusters (cyan circles). Their dwell lifetimes are also shown (**Extended Data Fig. 1m**).

h, Conventional and PALM super-resolution images (Voronoï diagram) of talin on the apical PM. The areas surrounded by the green curve (image in the middle) were the regions with good focus (the apical PM is tilted variously) and used for further analysis. The cyan lines in the image on the right indicate the smallest polygon that included the clustered spots.

i, Distributions of the cluster diameters.

j, Distributions of the molecule copy number in a cluster (compare with the data in **c**).

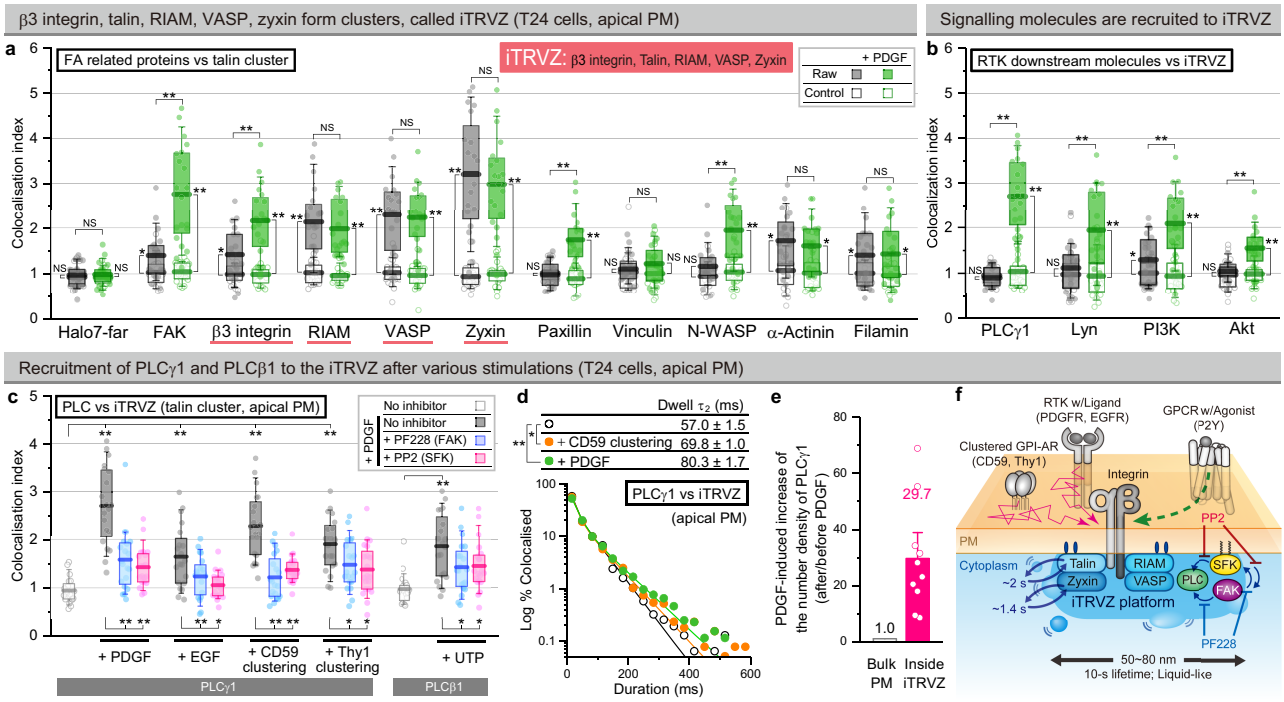

Figure 2 | iTRVZ works as the signalling platform for various signalling pathways.

a, Colocalisation indices of various FA proteins with talin clusters. In the box plots throughout this report, bars, boxes, and whiskers indicate mean values, interquartile range (25–75%), and 10–90% range, respectively.

b, Colocalisation indices of the signalling molecules downstream of PDGFR with iTRVZ.

c, Colocalisation indices of PLCγ1 and PLCβ1 with iTRVZ after various stimulations, and the effects of FAK and SFK inhibitors.

d, Dwell time of PLCγ1 on iTRVZ; prolonged after stimulations (for τ_2, see the caption to **Fig. 1**).

e, PDGF-induced increases of the PLCγ1 number density (after/before PDGF) outside (bulk) and inside iTRVZ (dots for individual cells and mean ± SEM).

f, Schematic drawing summarising the characteristic properties of iTRVZ.

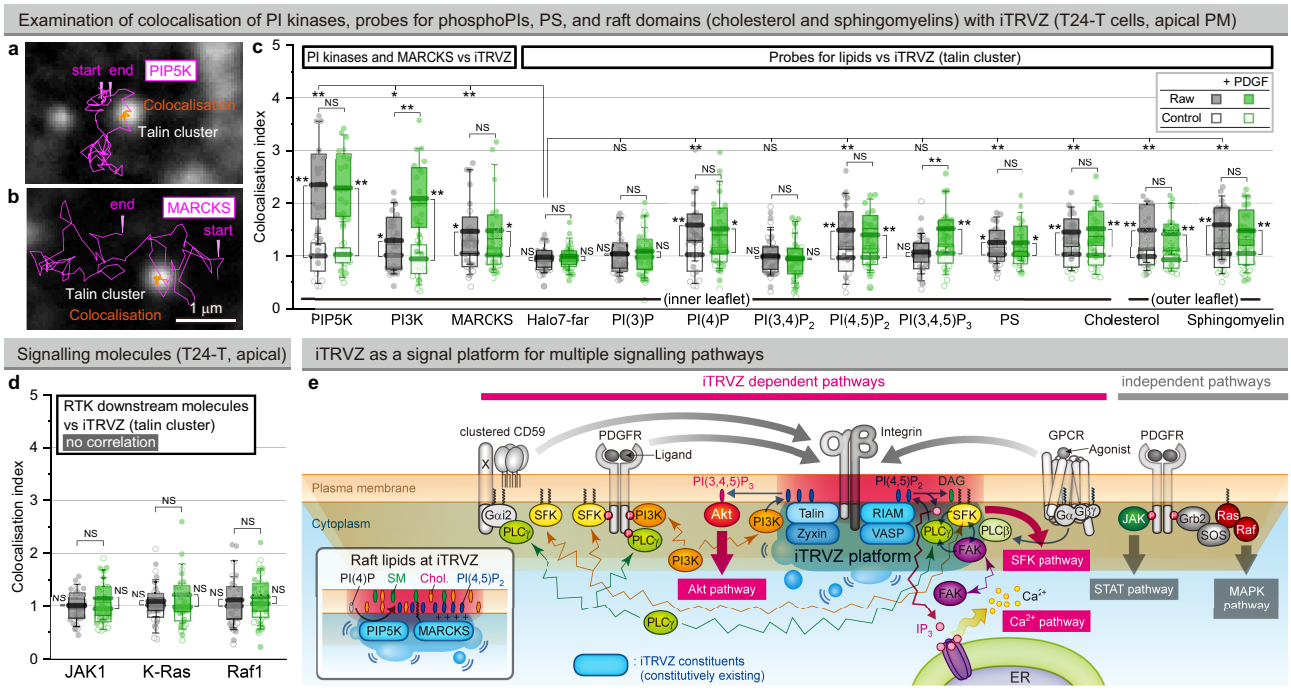

Figure 3 | PI kinases, some phosphoinositides, PS, and raft domains are colocalised with iTRVZ.

a, **b,** PIP5K (**a**) and MARCKS (**b**) (trajectories) became transiently colocalised with talin clusters (white spots) (**Supplementary Video 6**).

c, Colocalisation indices of PI kinases and lipid-binding probes with iTRVZ (data for PI3K are the same as those in **Fig. 2b**).

d, Colocalisation indices of JAK1, K-Ras, and Raf1 with iTRVZ (no correlation).

e, Schematic diagram summarising various signalling processes occurring at iTRVZ.

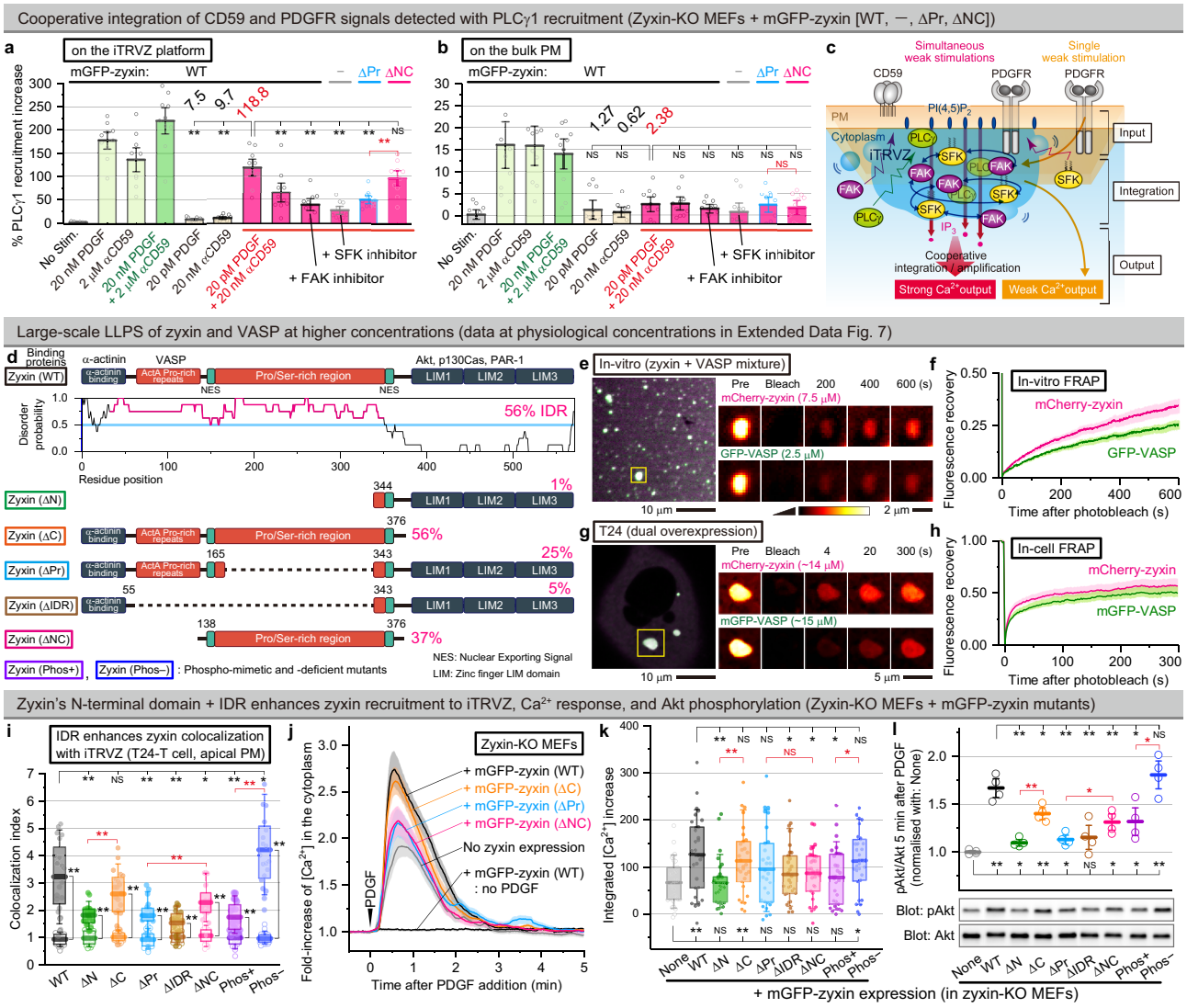

Figure 4 | iTRVZ works as a cooperative signal integrator and forms with the aid of LLPS by IDR interactions.

a, b, % Increases of the total number of recruited PLCγ1 on iTRVZ (**a**) and the bulk PM (**b**) after separate and simultaneous CD59 and PDGFR stimulations.

c, Schematic figure showing that iTRVZ non-linearly integrates the CD59 and PDGFR signals by inducing cooperative interactions of FAK and SFK (**Extended Data Fig. 5e**).

d, Domain structures of zyxin and its mutants used (predicted IDR in magenta).

e-h, *In-vitro* (**e, f**; 10 min after 1% PEG8K addition) and in-cell (**g, h**) FRAP of zyxin and VASP co-clusters (**Supplementary Video 7**).

i, Colocalisation indices of zyxin mutants with iTRVZ.

j, k, Ca^{2+} mobilisation after PDGF stimulation. Typical time courses (**j**) and total Ca^{2+} signals (**k**).

l, Western blot analysis of PDGF-induced Akt phosphorylation.

Methods

Cell culture and transfection

T24 cells, a kind gift from Masahiro Sokabe (Nagoya University)[43], HeLa cells, purchased from the RIKEN Cell Bank (RCB0007), and CHO-K1 cells, purchased from Dainippon Pharma Co., Ltd., (03-402), were cultured in Ham's nutrient mixture F12 (Sigma Aldrich: N6658) supplemented with 10% (vol/vol) fetal bovine serum (FBS, Gibco: 10270-106, Lot#: 42G7281K). The talin1 and 2 double knockout mouse embryonic fibroblasts (talin-dKO MEFs) and talin2-KO MEFs, kind gifts from Reinhard Fässler (Max Planck Institute of Biochemistry)[11], the zyxin-KO MEF line, a kind gift from Mary C. Beckerle (University of Utah)[13], the control MEF lines 1-3, kind gifts from Noboru Mizushima (University of Tokyo), the control MEF line 4, a kind gift from Ryusuke Kuwahara (Okinawa Institute of Science and Technology Graduate University), and the NIH3T3 cell line, a kind gift from Makoto Kinoshita (Nagoya University)[44], were cultured in Dulbecco's modified Eagle's medium (DMEM, Sigma Aldrich: D5796) supplemented with 10% (vol/vol) FBS, 100 U/ml penicillin, and 100 μg/ml streptomycin (Nacalai Tesque: 26253-84). The mouse embryonic stem cells (mESCs, clone E14tg2a), purchased from the RIKEN Cell Bank (AES0135, Lot#: 2)[45], were cultured in DMEM supplemented with 15% (vol/vol) embryonic stem-cell qualified FBS (Gibco: 16141079), 1x MEM non-essential amino acids solution (Gibco: 11140050), 1 mM sodium pyruvate (Gibco: 11360070), 55 μM 2-mercaptoethanol (Gibco: 21985023), 100 U/ml penicillin, 100 μg/ml streptomycin, and 10^3 U/ml mouse leukemia inhibitory factor (LIF, Millipore: ESG1106) without feeder cells[46]. The identities of the T24 and HeLa cell lines were authenticated by PowerPlex16 STR (contracted to Promega). All of the cells used were mycoplasma free, as determined by using MycoAlert (Lonza: LT07-118) and a Mycoplasma PCR Detection Kit (Beyotime Biotechnology: C0301S). The transfection of cells with the plasmid vectors was performed by electroporation with a Lonza 4D-Nucleofector, according to the manufacturer's recommendations, using the SF solution and program EN138 for T24 and NIH3T3 cells; SE and CN114 for HeLa cells; SF and DT133 for CHO-K1 cells; SE and DS150 for talin-dKO MEFs; SF and CZ167 for other MEFs; and SF and CG104 for mESCs.

For the generation of cell lines stably expressing selected proteins, the cells were transfected with the expression vector (for the pPBpuro expression vector, pCMV-mPBase was co-transfected). Two days after transfection, the cells were selected by an incubation with G418 (800 μg/ml for T24, 1,000 μg/ml for MEFs) or puromycin (0.5 μg/ml for T24, 1 μg/ml for MEFs). After an incubation in the selection medium for a week, the cell lines were cloned by limiting dilution using 96-well

plates. The expression levels of isolated cell clones were examined by western blotting and immunofluorescence microscopy. The established stable cell lines were routinely cultured in the presence of antibiotics.

For fluorescence microscopy, the cells were plated in a glass-bottom dish with a glass window size of 12 mm in diameter (No.1S, Iwaki: 3971-035), pre-coated with fibronectin (FN, Sigma Aldrich: F1141) by placing 100 µl of 10 µg/ml FN in phosphate buffered saline (PBS: 137 mM NaCl, 8.1 mM $NaHPO_4$, 2.7 mM KCl, 1.5 mM KH_2PO_4, pH 7.4) on the glass at room temperature (RT) for 30 min. The cells were cultured in the complete growth medium for 24–48 h before use. For cell stimulation experiments using epidermal growth factor (EGF) and platelet-derived growth factor (PDGF), the cells were pretreated with the FBS-free medium for 3-12 h. For microscope observations, the medium was replaced by Hanks' balanced salt solution (Nissui: 05905) buffered with 2 mM TES (Dojindo: 348-08371) at pH 7.4 (observation medium; T-HBSS).

For the expression of the CRY2 protein, transfected talin1/2-dKO MEFs were first incubated in the complete growth medium at 37ºC for 2 h for recovery from the transfection, and then cultured at 33ºC for 2 days, to allow for better folding of the CRY2 protein, followed by the incubation at 37ºC for 3 h before microscope observations.

Cell stimulation

CD59 and Thy1 were activated by polystyrene beads coated with the respective monoclonal antibodies. Mouse anti-CD59 and mouse anti-Thy1 monoclonal antibodies were purified from the culture media of hybridoma MEM43/5 (a kind gift from Vaclav Horejsi [Institute of Molecular Genetics of the Czech Academy of Sciences])[47] and hybridoma OX7 (European Collection of Cell Cultures: 84112008)[48,49], respectively. The carboxylate-modified yellow-green or dark-red fluorescent 40-nm polystyrene beads (Molecular Probes: F8795, F8789, respectively; final concentration of 0.4 µM) were functionalised by incubating them at RT for 10 min in the activation solution, containing 2 mM 1-ethyl-3-(3-dimethylaminopropyl)carbodiimide (EDC, Pierce: 22980), 4 mM sulfo-N-hydroxysuccinimide (sulfo-NHS, Pierce: 24525), and 150 mM NaCl, buffered with 0.1 M 2-(N-morpholino)ethanesulfonic acid (MES) at pH 5.5. Afterwards, a 9 µl portion of the antibody (1 mg/ml in PBS) was mixed with 3 µl functionalised beads, 3 µl borate -buffered saline (150 mM NaCl buffered with 0.5 M borate [Wako: 021-02195] at pH 8.0), and 1 µl 0.4 M NaOH. After an incubation at RT for 1 h, the coupling reaction was stopped by the addition of 7.5 µl of 300 mM glycine and 1 µl of 5% polyethylene glycol with a mean molecular weight of 20,000 (PEG20K, Sigma Aldrich: P5413) in PBS and incubated at RT for 5 min. The mixture was ultracentrifuged (50,000 rpm for 15 min), and then the antibody-coated beads were resuspended in 1 ml PBS containing 0.1% PEG20K, ultracentrifuged again, and resuspended in T-HBSS containing 2%

bovine serum albumin (BSA, Sigma Aldrich: A3059) and 0.1% PEG20K. Right before use, the bead suspension was sonicated for 5 min, followed by centrifugation (15,000 rpm for 10 min). The cells were first incubated in T-HBSS containing 0.5% BSA and 0.1% PEG20K, and then the bead suspension was added at a final concentration of 2 μM or 20 nM. The observations were finished within 10 min after the bead addition to avoid the effect of internalisation.

Stimulations of the receptor-type kinases (RTKs) were performed by incubating the cells with 20 nM human recombinant EGF (Wako: 053-07871), 20 nM or 20 pM human recombinant PDGF-BB (Pepro Tech: 100-14B), and 100 μM uridine triphosphate (UTP, Invitrogen: R0471). All microscope observations were finished within 5 min after the stimulation.

Cell treatments with various reagents

The kinase activity of Src family kinases (SFKs) was inhibited by treating the cells with 10 μM PP2 (Selleckchem: S7008)[50] at 37°C for 10 min. The kinase activity of focal adhesion kinase (FAK) was inhibited by treating the cells with 10 μM PF573228 (Cayman Chemical: 14924)[51] at 37°C for 10 min.

Partial actin depolymerisation was performed by incubating the cells in medium containing 100 nM latrunculin A (Wako: 125-04363), 500 nM cytochalasin D (Cayman Chemical: 11330), or 10 μM Y27632 (ChemScene: CS-0878) for 10 min at 37°C. Partial depletion of cholesterol was achieved by incubating the cells in 4 mM methyl-β-cyclodextrin (MβCD, Sigma Aldrich: 332615) at 37°C for 30 min or in 60 μg/ml saponin (Nacalai Tesque: 30502-42) on ice for 15 min[38]. Replenishment of cholesterol was performed by incubating the cholesterol-depleted cells in 10 mM MβCD-cholesterol complex (1:1 mol/mol; Sigma Aldrich: C3045) at 37°C for 30 min[38]. Partial depletion of PI(4,5)P_2 from the PM was performed by incubating the cells with 10 μM ionomycin (Wako: 093-04531) at 37°C for 5 min[52], 1 μM phenylarsine oxide (Tokyo Chemical Industry: P0140) at 37°C for 3 h, or 50 μM quercetin (Sigma Aldrich: Q4951) at 37°C for 3 h[25,53].

To inhibit the interactions between the intrinsically disordered regions (IDRs) of the proteins, cells were first lightly permeabilised with 1% Tween 20 in T-HBSS at RT for 10 min, and then treated with T-HBSS containing 5% 1,6-hexanediol (Wako: 081-00435) on the microscope stage during observation. The microscope observations were finished within 10 min[54]. For *in vitro* experiments, 1,6-hexanediol was added at a final concentration of 10%.

cDNA construction

All plasmids used in this study are listed in the **Supplementary Table**, and the complete plasmid sequences in the GenBank format with annotations are shown in the **Supplementary Data**. The cDNAs encoding SNAPf, Halo7, mEGFP, and mCherry were obtained from New England Biolabs

(N9172S), Promega (G9651) and Clontech (Z2370N, Z2522N), respectively. The cDNA encoding mEos3.2 was generated by making 3 point-mutations, I102N, H158E, and Y189A, in the Addgene mEos2 plasmid (#20341), a kind gift from Loren L. Looger (Janelia Research Campus)[55–57]. The cDNAs encoding the deletion mutants of RIAM, VASP, and zyxin were generated by PCR with designed primers. The cDNAs encoding phosphomimetic and phosphodeficient mutants of zyxin and VASP were custom synthesised by Gene Universal. The cDNAs encoding mScarlet-I[58], domain 4 from perfringolysin O with the D434S mutation (D4H)[59,60], and ostreolysin A with the E69A mutation (OlyA [E69A])[23] were custom synthesised by Sangon Biotech (Shanghai, PRC).

The cDNAs encoding the following proteins were kind gifts from researchers. Mouse FAK (Caroline H. Damsky, University of California, San Francisco)[61]; human RIAM (Chinten J. Lim, University of California, San Diego)[62]; human β3 integrin (Jonathan C. Jones, Northwestern University)[63]; rat N-WASP (Jack Taunton, University of California, San Francisco)[64]; mouse PIP5KIγ (Richard A. Anderson, University of Wisconsin)[65]; probes for PI(4)P, PI(3,4)P_2, PI(4,5)P_2, and PI(3,4,5)P_3 (Toshiki Itoh, Kobe University)[21]; a probe for phosphatidylserine (Tomohiko Taguchi, Tohoku University)[27,66]; CIBN and CRY2-5ptase (Pietro de Camilli, Yale University)[24]; human CD59 (Masahide Tone, Oxford University)[67]; rat Thy1 (Roger J. Morris, King's College London)[48]; human PDGFR-β (William Hahn, Broad Institute of MIT and David Root, Harvard University)[68]; rat PLCγ1 (Matilda Katan, Cancer Research UK Centre)[69]; mouse PLCβ1 (Katsuhiko Mikoshiba, ShanghaiTech University)[70]; human K-Ras and human Raf1 (Akihiko Yoshimura, Keio University)[71]; and human CD47 (Eric C. Brown, Genentech)[72].

The five-amino acid linker sequence (Ser-Gly-Gly-Gly-Gly) was inserted between the target protein and mGFP, mCherry, and mScarlet-I, and the 15-amino acid linker ((Ser-Gly-Gly-Gly-Gly)$_3$) was inserted between the target protein and SNAPf, Halo7, and mEos3.2.

The sequences encoding various proteins were subcloned into the following vectors: pEGFP, pmCherry (Clontech: Z2370N, Z2522N), pET26B (Novagen: 69862), and pPBpuro (a custom vector with the PiggyBac terminal repeat sequence and the high expression promoter consisting of chicken beta actin promoter, CAG promoter with an artificial intron, and CMV IE, a kind gift from Michiyuki Matsuda, Kyoto University)[73]. pCMV-mPBase was a kind gift from Michiyuki Matsuda (Kyoto University)[73].

Western blotting

Ice-cold radio immunoprecipitation assay (RIPA) buffer, consisting of 150 mM NaCl, 5 mM ethylenediaminetetraacetic acid (EDTA, Dojindo: 345-01865), 1% NP-40 (Wako: 141-08321), 1% sodium deoxycholate (Nacalai Tesque: 08805-72), 0.1% sodium dodecyl sulfate (SDS, Wako: 191-07145), and 100x diluted protease inhibitor cocktail (Nacalai Tesque: 25955-24), buffered with 50

mM tris(hydroxymethyl)aminomethane (Tris)-HCl at pH 7.4 (350 µl) (100x diluted phosphatase inhibitor cocktail [Nacalai Tesque: 07574-61] was included for the Akt phosphorylation assay), was added to cells cultured to ~80% confluency in a 60-mm plastic dish, and kept on ice for 5 min. The entire material in the dish was collected by using a cell scraper, and then centrifuged at 15,000 rpm for 20 min. The supernatant (300 µl) was mixed with 100 µl of 4x Laemmli sample buffer, consisting of 8% SDS, 0.12% bromophenol blue, 40% glycerol, and 400 mM dithiothreitol, buffered with 200 mM Tris-HCl at pH 6.8, and boiled for 5 min. The boiled mixture (2 ~10 µl, 1~2 µg of total protein for each lane) was loaded on a precast 4-20% gradient polyacrylamide gel (PAGE, Bio-Rad: 4561096) and electrophoresed at a constant voltage of 200 V for 35 min, using a Mini Protean Tetra Cell (Bio-Rad: 1658000JA), in Tris-glycine running buffer (25 mM Tris-HCl, 190 mM glycine, and 0.1% SDS). The direct addition of the 4x Laemmli buffer to the cells gave virtually the same results, but the background of the western blot membrane was higher, and thus we performed the initial cell solubilisation with the RIPA buffer.

The proteins separated by SDS-PAGE, zyxin, VASP, and Akt, were blotted onto polyvinylidene fluoride (PVDF) membranes by the semi-dry transfer method, using a Trans-Blot Turbo (Bio-Rad: 1704150, mixed MW protocol) with the PVDF transfer pack (Bio-Rad: 1704156). In the case of talin, the wet transfer to the PVDF membrane (Immobilon-P, Millipore: IPVH00010) was performed using a running buffer containing 25 mM Tris-HCl, 190 mM glycine, and 20% methanol at 4ºC, with a constant voltage of 100 V for 1 h (Mini Protean Tetra Cell). The immuno-detection was performed by a SNAP i.d. (Millipore, SNAP2BASE), according to the manufacturer's recommendations. The membranes were blocked with Blocking One (Nacalai Tesque: 03953-95) and washed with Tris-buffered saline (TBS; 137 mM NaCl and 2.7 mM KCl buffered with 25 mM Tris-HCl, pH 7.4) supplemented with 0.1% Tween 20 (TBS-T).

Primary antibodies were as follows: mouse anti-talin1 (clone 93E12, Abcam: ab104913, Lot#: GR24449-3, 0.5 µg/ml), rabbit anti-zyxin (B71, Millipore: ABC1463, Lot#: Q3027780, 4,000x dilution), rabbit anti-GFP (ProteinTech: 50430-2-AP, Lot#: 78456, 0.5 µg/ml), rabbit anti-VASP (clone 9A2, Cell Signaling Technology: 3132, Lot#: 5, 21 ng/ml), rabbit anti-Akt (Cell Signaling Technology: 9272, Lot#: 5, 17 ng/ml), rabbit anti-phospho-Akt (pS473, clone D9E, Cell Signaling Technology: 4060, Lot#: 25, 48 ng/ml), mouse anti-GAPDH (ProteinTech: 60004-1-Ig, Lot#:10008047, 10 ~ 500 ng/ml). Secondary antibodies were the following: horseradish peroxidase (HRP)-conjugated goat anti-mouse immunoglobulin G (IgG, Invitrogen: G21040, Lot#:2122350, 0.5 µg/ml) and HRP-conjugated goat anti-rabbit IgG (Invitrogen: G21234, Lot#:2087715, 0.5 µg/ml).

The membrane was then incubated with Western BLoT Hyper HRP Substrate (Takara: T7103B) for chemiluminescence detection, and then imaged with an LAS-3000 (Fuji Film, high

sensitivity mode) or iBright FL1500 (Thermo Fischer Scientific, 2x2 binning, 1.5x zoom) image analyser. Quantitative analysis of the protein bands was performed with the ImageJ software. The signal intensities were normalised by the GAPDH intensities. To measure the phosphorylation of Akt, the membrane was first treated and imaged to measure Akt phosphorylation, and then the bound antibodies and the chemifluorescent product were removed by incubating the membrane with stripping buffer, consisting of 2% SDS and 100 mM 2-mercaptoethanol buffered with 62.5 mM Tris-HCl at pH 6.7, at 50ºC for 20 min, followed by reprobing with the anti-Akt antibodies.

Cell attachment assay

Cultured cells (in 100-mm plastic dishes, ~80% confluence) were detached with a freshly prepared trypsin solution (0.25% trypsin and 1 mM EDTA in PBS) at RT for 3 min. After brief centrifugation (1,000 rpm for 3 min), the cells were resuspended in the complete growth medium, and the cell number was determined with a hemocytometer. The cell concentration was adjusted to 3 x 10^4 cells/ml and the cells were incubated in the CO_2 incubator at 37ºC for 30 min, for recovery from the detachment process. Afterwards, 1 ml of the cell suspension was dispensed into each FN-coated well in the 12-well plastic plate, which was then placed in the CO_2 incubator for 5 min. The plate was then gently washed twice with T-HBSS, and the cells were imaged by a ZEISS Primovert Photo inverted phase-contrast microscope. The numbers of attached cells were counted by the ImageJ software.

Fluorescence labelling of molecules

To fluorescently label the SNAPf and Halo tags bound to target proteins expressed in cells, the cells were incubated at 37ºC in complete growth medium containing either 50 nM SNAP-tetramethylrhodamine (TMR) star (New England BioLabs: S9105S) for 60 min, or 20 nM TMR-Halo linker (Promega: G8251), 20 nM SaraFluor650T Halo linker (SF650, Goryo Chemical: A308-02), or 100 nM JF646 Halo linker (Promega: GA1120) for 30 min. The labelling efficiencies (including the misfolding, slow folding, and cleavages of the tag proteins) were estimated to be 66 ± 1.8% for SNAPf, 88 ± 2.2% for Halo7, and 76 ± 2.3% for mEGFP, using the control monomeric molecules mGFP-CD47-SNAPf and mGFP-CD47-Halo7 (SNAPf and Halo7 tags located in the cytoplasm).

Immunofluorescence labelling

The cultured cells on the FN-coated glass-base dish were fixed with cold methanol (-20ºC) for 5 min for talin staining or 4% paraformaldehyde for 1 h for zyxin staining. The fixed cells were incubated at RT with 100 mM glycine for 15 min, 0.1% Triton X-100 for 5 min, and then 1% BSA

for 1 h (all solvents were PBS containing 0.1% Tween 20; PBS-T). The cells were immunostained by sequential 1 h incubations with primary and secondary antibodies at RT. Each incubation was followed by three washes with PBS-T.

The following antibodies were used: mouse anti-talin1 (clone 97H6, Bio-Rad: MCA4770, Lot#:1803, 1 μg/ml), rabbit anti-zyxin (B71, Millipore:ABC1463, Lot#: Q3027780, 600x dilution), Rhodamine Red-X-conjugated donkey anti-mouse IgG (Jackson: 715-295-150, Lot#: 145566, 1 μg/ml), and Rhodamine Red-X-conjugated donkey anti-rabbit IgG (Jackson: 711-295-152, Lot#: 145693, 1 μg/ml).

Single fluorescent-molecule imaging and analysis

All single-molecule observations were performed at 37°C, using a microscope housed in a home-made environmental chamber. Fluorescently labelled molecules in cells were excited by total internal reflection (TIR) illumination (for those on the basal PM) or oblique-angle illumination (for those on the apical PM) using objective-lens-type TIRF microscopes, which were constructed on Olympus and Nikon inverted microscopes (IX-83 and TiE, respectively) equipped with 100x 1.49 NA objective lenses (UApoN100XTIRF and ApoTIRF100XC, respectively). The two-colour fluorescence images were separated into the two detection arms of the microscope by a dichroic mirror (Chroma: ZT561rdc-UF3 or ZT640rdc-UF3). The detection arms were equipped with band-pass filters of ET525/50m, ET600/50m, or ET700/75m (all from Chroma), and the images were recorded at each arm with a two-stage microchannel plate intensifier (Hamamatsu Photonics: C9016-02MLP24), lens-coupled to a scientific complementary metal oxide semiconductor (sCMOS) camera (ORCA-Flash ver4.0 V2 plus, Hamamatsu Photonics: C11440-22CU). The final magnifications were 133 and 100x, resulting in pixel sizes of ~50 and 65 nm (square pixels), respectively.

The incident excitation laser powers at the sample plane for single molecule observations with the oblique illumination were 0.29 $\mu W/\mu m^2$ for the 488-nm line (for mEGFP, Coherent: OBIS 488-100 LS), 0.21 $\mu W/\mu m^2$ for the 561-nm line (for TMR, Coherent: OBIS 561-100 LS), and 0.37 $\mu W/\mu m^2$ for the 642-nm line (for SF650 and JF646, Omicron: LuuXPlus 640-140). For the TIRF illumination, we employed very shallow angles and 2x-increased incident laser powers. Under these conditions, the photobleaching lifetimes for fluorophores on the apical PM with the oblique-angle illumination (basal PM with the TIR illumination) were the following: mEGFP, 0.61 ± 0.02 (0.74 ± 0.02) s; SNAPf-TMR, 3.65 ± 0.15 (3.68 ± 0.18) s; Halo7-TMR, 8.87 ± 0.47 (9.50 ± 0.48) s; Halo7-SaraFluor650, 12.69 ± 0.57 (14.38 ± 0.53) s; and Halo7-JF646, 11.12 ± 0.62 (12.01 ± 0.54) s. For the cluster (iTRVZ) observations, the laser powers were reduced by a factor of three from those used for single molecule observations. The dual-colour images were separated by a dichroic mirror

(Chroma: ZT561rdc-UF3 or ZT640rdc-UF3) and projected into two detection arms with band-pass filters of ET525/50m, ET600/50m, or ET700/75m (all from Chroma).

Each individual fluorescent spot in the image was identified and tracked by using an in-house computer program, as described previously[14,56,57,74]. The superimposition of images in different colours obtained by two separate cameras was conducted as described previously[75].

Transient-immobilisation events, called Temporary Arrest of LateraL diffusion (TALL[76,77]), were detected in single-molecule tracking trajectories, by using the algorithm developed[78] and modified[76,77] previously. The detection circle radius and the threshold residency time were set at 200 nm and 5 frames (0.167 s), respectively. The cluster lifetimes and molecular dwell lifetimes on iTRVZ should in principle be corrected for the photobleaching lifetimes of the probes[77], but since the observed durations were much shorter than the probes' photobleaching lifetimes, no corrections were performed.

Colocalisation index analysis

To quantitatively measure the colocalisation of single molecules with iTRVZ clusters (talin and zyxin clusters), since the sizes of the cluster images are virtually the size of the light diffraction limit (they appear like single-molecule spots in terms of their sizes), we employed a "colocalisation index" parameter, based on the pair cross-correlation analysis for single-molecule movies simultaneously recorded in two colours (such as green and red)[17,79], as shown in **Extended Data Fig. 3k**. Briefly, (1) a region of interest (ROI) is selected, and then the distances between all pairs of green and red spots in the ROI in a video frame are measured, and this is repeated for all of the video frames in an image sequence. (2) The distribution of the number of distances R(r) is plotted against the distance. The normalisation factor $N(r)$ is computed using fast Fourier transform, as described[17,79]. (3) The cross-correlation function $C(r)$ is calculated by dividing $R(r)$ by $N(r)$. (4) The colocalisation index is defined as the ratio of the value of the pair correlation function between 0 and 50 nm and the value between 450 and 500 nm. When no significant colocalisation exists, the colocalisation index is 1, and with an increase of colocalisations, the index increases. The control data without any correlation between green and red spots were produced by shifting each spot in the image by 1 μm in random directions.

PALM observation and analysis

Cells expressing the proteins conjugated with mEos3.2 were chemically fixed for PALM observations. Briefly, cells were initially fixed with 0.3% (v/v) glutaraldehyde in cytoskeleton buffer (150 mM NaCl, 5 mM EGTA, 5 mM glucose and 5 mM $MgCl_2$, buffered with 10 mM MES at pH 6.1) containing 0.25% (v/v) Triton X-100 for 1 min, and then post-fixed with 2% (v/v)

glutaraldehyde in the same solution for 15 min[80]. The cells were then incubated with freshly prepared 0.1% (w/v) sodium borohydride for 7 min to quench the unreacted aldehyde groups. After replacing the cytoskeleton buffer with T-HBSS, the fixed cells were observed at 37°C by a home-built PALM station.

The PALM station is virtually the same objective-lens-type TIRF microscope developed for single-molecule imaging, based on an Olympus IX-83. The samples were illuminated with the TIR or oblique-angle illumination mode, using an activation laser (405-nm, Cobolt: 06-MLD 405-100; increased from 1.5 to 78 nW/μm^2 on the sample plane following the Fermi photoactivation scheme [t_F = 162, T = 16.2 s][81]), an excitation laser (561-nm, MPB Communications: Fiber 560-20000; 12.4 μW/μm^2), and an additional weak 488-nm laser to suppress the long-lived dark state[82] (Coherent: Sapphire 488-300 CW; 0.164 μW/μm^2). The PALM data acquisition was performed at 60 Hz for 14,560 frames with an image size of 512 x 512 pixels, using the high-speed camera system (Photron: mini AX200-II) described previously[56,57]. The final magnification was 250x (~80 nm/pixel; square pixels).

The detection of the spots in the images was performed by using the ThunderSTORM plugin of ImageJ[83] with "Wavelet filtering" (B-Spline order = 3 and B-Spline scale = 2.0) and the "Local maximum method" (Peak intensity threshold = 30 ~ 50 and Connectivity = 8-neighborhood). After the spot detection, the post-processing steps of "Remove duplicates" (Distance threshold = uncertainty) and "Drift correction" (cross-correlation with 5 bins) were further performed. These datasets were imported to the SR-Tesseler software[16] for the cluster analysis and image reconstruction. First, the areas with good focus in the apical PM and those that do not contain obvious FAs were selected as ROI. Second, blinking and multi-ON frame detections were corrected by the "Detection cleaner" function using the following parameters: photon/background size = 0.3; fixed maximal dark time = 200; intensity to photon ratio = 0.039; and background value = 0.3 (**Extended Data Fig. 2a**)[82]). Third, cluster contour detection was performed by using a Voronoï polygon density factor of 3.5 (within the whole ROI).

Confocal microscopy and FRAP

To obtain confocal fluorescence images of the cells at 37ºC, we employed a custom-built spinning-disk confocal microscope based on an Olympus IX83 (placed in a home-built environmental chamber) equipped with an Olympus objective PLXApo60XO or UApoN100XTIR, a Yokogawa confocal unit, CSU-W1, and a Hamamatsu Photonics ORCA-Flash 4.0 V2 plus sCMOS camera.

For the in-cell fluorescence recovery after photobleaching (FRAP) experiments, we employed a Nikon A1R confocal microscope equipped with a stage top incubator (Tokai hit, STXG-TIZWX-SET) operated at 37ºC, with recordings at 0.5 Hz. The photobleached-observed area was a circular

region of ~1 μm in diameter, and photobleaching was performed by illuminating the area with a 488 or 561 nm laser beam at 30% of the full laser power for ~1 s. For the *in vitro* FRAP experiments, a mixture of purified proteins was diluted with the observation buffer (150 mM NaCl and 0.5 mM tris(2-carboxyethyl)phosphine) [TCEP] buffered with 25 mM Tris–HCl, pH 7.4). After the addition of a final concentration of 1% PEG8K (Sigma Aldrich: P5413), the mixed solution was placed on the glass-bottom slide (Ibidi: 81507) and observed at 37ºC and 1 Hz by a Nikon spinning-disk confocal microscope, consisting of a Nikon TiE inverted microscope, a Nikon PlanApo 60x/1.40 objective lens, a Yokogawa CSU-X confocal unit, an Andor Revolution SD System, an Andor iXon 888-U3ultra camera, and an OkoLab stage top incubator. The photobleached-observed area was a circular region of ~1.5 μm in diameter, and photobleaching was performed by illuminating the area with a 488 nm laser beam (3.9 mW) for 0.5 s. The intensity recovery traces were analysed (background corrected and normalised) by the Image J software, based on the previously described method[84].

Cell volume measurement

The cells were transfected with the plasmid encoding SNAPf (without any fusion proteins), and plated on the FN-coated glass-bottom dishes. After culturing for 48 h, the expressed SNAPf proteins were labelled with 20 nM SNAP-TMR star at 37ºC for 30 min. After washing three times with T-HBSS, the medium was replaced with 1,000x diluted NucSpot Live 650 (Biotium, 40082) in T-HBSS for nuclear staining. Without washing, the whole 3D cell images were captured by Z scanning (250 nm pitch) with an Olympus custom-built spinning-disk confocal microscope.

The obtained images were binarised by the ImageJ software with Otsu's binarisation algorithm[85]. The volumes of the whole cell and the nucleus were determined from the binarised images of SNAPf and NucSpot Live 650, respectively, by counting the total voxel numbers. The volume of the cytoplasm was calculated by subtracting the nucleus volume from the whole cell volume.

Measurements of intracellular Ca^{2+} concentrations

The cells were incubated with 20 μM CalBryte 590 (AAT Bioquest: 20700) in T-HBSS at 37ºC for 30 min, and then washed three times with T-HBSS. The cells were observed at 37ºC by a home-built objective-lens-type TIRF microscope (Nikon TiE-base) equipped with a Nikon Plan Fluor 20x/0.50 objective lens. The cells were illuminated by a 561 nm laser at the Epi angle at a laser power of 0.22 nW/μm^2 on the sample. Recordings were performed at 1 or 2 Hz. To avoid the incorporation of CalBryte 590 in endosomes by endocytosis, all observations were finished within 1 h after labelling.

Protein purification

For preparing the cholesterol probe (Halo7 tag fused to D4H[59,60]) and sphingomyelin probe (Halo7 tag fused to OlyA(E69A)[23]), BL21 (DE3) *E. coli* competent cells (New England BioLabs: C2527) were transfected with the expression plasmids by heat shock, and then cultured at 37˚C in Luria-Bertani medium containing 50 μg/ml kanamycin, with agitation until the optical density at 600 nm reached 0.4 ~ 0.6. The cells were further cultured with 0.6 mM isopropyl-β-D-thiogalactopyranoside (Amresco: MFCD00063273) at 24˚C for 12 h. The cells were collected by centrifugation at 7,000 rpm for 3 min, resuspended in lysis buffer (1% Triton X-100 and 300 mM NaCl buffered with 20 mM Tris-HCl, pH 8.0) containing the protease inhibitor cocktail (Nacalai Tesque: 25955-24), and then disrupted by agitation on ice for 20 min. The suspension was centrifuged at 12,000 rpm for 10 min, and the supernatant was filtered through a Millex filter (0.45 μm pore; Millipore: SLFH05010) to remove the cell debris. The filtered solution was loaded on a column packed with nickel-nitrilotriacetic acid (Ni-NTA) agarose beads (Sangon Biotech: C600332-0001), and the bound proteins were eluted by the sequential additions of 10 mM (10 ml), 20 mM (10 ml), and 30 mM (5 ml) imidazole (all in 150 mM NaCl buffered with 20 mM Tris-HCl, pH 8.0), and finally, of 10 mM imidazole in 250 mM NaCl buffered with 20 mM Tris-HCl, pH 8.0 (10 ml). The eluted fractions were desalted and concentrated with an Amicon Ultra concentrator (10 kDa cutoff, Millipore, UFC501008) with 150 mM NaCl buffered with 20 mM 4-(2-hydroxyethyl)-1-piperazine ethanesulfonic acid (HEPES), pH 7.4. The probe concentrations were determined according to the optical absorbance at 280 nm, assuming molecular extinction coefficients of 1.02 and 0.977 x 10^5 (M/cm) for Halo7-D4H and Halo7-OlyA(E65A), respectively (determined from the amino acid composition data[86]). To label probes with the SeTau647-Halo ligand[77], purified probes were incubated with 1.5 equivalents of SeTau647-Halo ligand at 37 ˚C for 3 h. The labelled proteins were separated from the unreacted ligand by Ni-NTA affinity column chromatography, followed by concentration-purification using an Amicon Ultra concentrator, according to the same protocol described for the initial purification of Halo7-D4H and Halo7-OlyA(E65A). Their purities were 71 and 90%, respectively, as determined by the Coomassie Brilliant Blue R-250 (CBBR, Fluka: 27816) staining of the SDS-PAGE gels. Aliquots (30 μl) of the labelled protein solutions were placed in Eppendorf tubes, rapidly frozen in liquid N_2, and stored at -80ºC until use.

For the preparation of zyxin (and its mutants) and VASP, the proteins were expressed as chimeric proteins with a 6xHis tag, maltose binding protein (MBP), Tobacco Etch Virus protease digestion sequence (TEV), mCherry (GFP for VASP), and zyxin (VASP) in Expi293F cells (Thermo Fisher Scientific: A14635) for three days. The cells were harvested and lysed by freeze-thawing in buffer A (200 mM NaCl, 1 mM EDTA and 0.5 mM TCEP buffered with 25 mM Tris-HCl, pH 7.4)

supplemented with protease inhibitor cocktail (cOmplete, ETDA-free, Roche: 11873580001) at RT. The lysates were centrifuged at 21,000g at 4ºC for 1 h, and then purified according to a two-step protocol. The first step was affinity purification on an MBP-binding dextrin Sepharose column (MPBTrap, GE Healthcare: 28-9187-78). The lysates were loaded twice on the column at a flow rate of 0.5 ml/min, and eluted with 10 mM maltose in buffer A at RT. The eluates were incubated with TEV protease (1:10 total protein weight) at 16ºC for 18 h to cleave the TEV sequence. The second step was the separation of mCherry-zyxin or EGFP-VASP from 6xHis-MBP and the removal of the His-tagged TEV protease by Ni-NTA chromatography (HisPur™ Ni-NTA Resin, Thermo Scientific: 88222). First, NaCl and imidazole were added to the digested solutions at final concentrations of 400 and 25 mM, respectively, and then the cleavage reaction solution was passed twice over a preequilibrated Ni-NTA Sepharose slurry (200 µl of bed volume, equilibrated with a buffer solution (300 mM NaCl, 25 mM imidazole, and 0.5 mM TCEP buffered with 25 mM Tris-HCl, pH 7.4), in a Poly-Prep Chromatography Column (Bio-Rad: 731-1550). The flow-through was collected and concentrated with a Pierce Protein Concentrator (30 kDa MWCO, PES-membrane, Thermo Scientific: 88502) to ~150 µl. The concentrated solutions were dialysed using micro-dialyser units (10 kDa MWCO, Slide-A-Lyzer MINI, Thermo Scientific: 69576) against buffer B (150 mM NaCl and 0.5 mM TCEP buffered with 25 mM Tris-HCl, pH 7.4) at 4ºC overnight. Finally, the concentrations of the proteins were determined using the absorbance at 280 nm, assuming molecular extinction coefficients of 6.11, 6.15, 5.30, 5.18, and 4.84 x 10^4 (M/cm) for GFP-VASP, mCherry-zyxin (WT), mCherry-zyxin (ΔPr), mCherry-zyxin (ΔIDR), and mCherry-zyxin (ΔNC), respectively (determined from the amino acid composition data[86]). The purities of GFP-VASP, mCherry-zyxin (WT), mCherry-zyxin (ΔPr), mCherry-zyxin (ΔIDR), and mCherry-zyxin (ΔNC) were 84, 72, 69, 89, and 71%, respectively, as determined by the staining of the SDS-PAGE gels with CBBR (InstantBlue Coomassie Protein Stain [ISB1L], Abcam: ab119211). Aliquots (10 µl) of the protein solutions were placed in Eppendorf tubes, which were rapidly frozen in liquid N_2 and stored at -80ºC until use.

In vitro phase separation assay

Purified zyxin and VASP solutions were diluted with buffer B to the desired protein concentrations. After the addition of 1% PEG8K, the mixtures were transferred to glass-bottom slides (Ibidi: 81507) for imaging. All reactions and observations were performed at 37ºC.

Software and statistical analysis

Superimpositions of image sequences obtained in two colours and tracking single-molecules in the movies were performed using C++-based computer programs produced in-house, as described

previously[74,75]. Conventional TIRF images were processed and analysed using Fiji[87] (NIH), MatLab 2019a (MathWorks), and ilastik[88]. Curve fittings were performed using Origin 2017 (OriginLab). Statistical analyses were performed using OriginPro 2017, Rstudio (with lawstat package), and Excel (Microsoft). $P<0.05$ was defined as statistically significant. Other image and data analyses were performed using Fiji and MatLab 2019a. Figures and videos were edited using Photoshop CC 2021 and Illustrator CC 2021 (Adobe).

Data availability

Source data are provided with this paper. All data generated or analysed for this study are available within the paper and its associated supplementary information files. All other data presented are available upon reasonable request from the corresponding author.

Code availability

All codes written for this study are available upon reasonable request from the corresponding author.

Methods references

43. Naruse, K., Sai, X., Yokoyama, N. & Sokabe, M. Uni-axial cyclic stretch induces c-src activation and translocation in human endothelial cells via SA channel activation. *FEBS Lett.* **441**, 111–115 (1998).

44. Ihara, M. *et al.* Association of the cytoskeletal GTP-binding protein Sept4/H5 with cytoplasmic inclusions found in Parkinson's disease and other synucleinopathies. *J. Biol. Chem.* **278**, 24095–24102 (2003).

45. Hooper, M., Hardy, K., Handyside, A., Hunter, S. & Monk, M. HPRT-deficient (Lesch–Nyhan) mouse embryos derived from germline colonization by cultured cells. *Nature* **326**, 292–295 (1987).

46. Xia, S. *et al.* Nanoscale architecture of the cortical actin cytoskeleton in embryonic stem cells. *Cell Rep.* **28**, 1251-1267.e7 (2019).

47. Štefanová, I. *et al.* Characterization of a broadly expressed human leucocyte surface antigen MEM-43 anchored in membrane through phosphatidylinositol. *Mol. Immunol.* **26**, 153–161 (1989).

48. Madore, N. *et al.* Functionally different GPI proteins are organized in different domains on the neuronal surface. *EMBO J.* **18**, 6917–6926 (1999).

49. Mason, D. W. & Williams, A. F. The kinetics of antibody binding to membrane antigens in solution and at the cell surface. *Biochem. J.* **187**, 1–20 (1980).

50. Hanke, J. H. *et al.* Discovery of a novel, potent, and Src family-selective tyrosine kinase inhibitor. *J. Biol. Chem.* **271**, 695–701 (1996).

51. Slack-Davis, J. K. *et al.* Cellular characterization of a novel focal adhesion kinase inhibitor. *J. Biol. Chem.* **282**, 14845–14852 (2007).

52. Kosenko, A. & Hoshi, N. A change in configuration of the calmodulin-KCNQ channel complex underlies Ca^{2+}-dependent modulation of KCNQ channel activity. *PLoS One* **8**, e82290 (2013).

53. Johnson, K. A. *et al.* PI(4,5)P_2 binding sites in the Ebola virus matrix protein modulate assembly and budding. *BioRxiv* 341248 (2018) doi:10.1101/341248.

54. Ulianov, S. V. *et al.* Suppression of liquid–liquid phase separation by 1,6-hexanediol partially compromises the 3D genome organization in living cells. *Nucleic Acids Res.* **49**, 10524–10541 (2021).

55. McKinney, S. A., Murphy, C. S., Hazelwood, K. L., Davidson, M. W. & Looger, L. L. A bright and photostable photoconvertible fluorescent protein. *Nat. Methods* **6**, 131–133 (2009).

56. Fujiwara, T. K. *et al.* Development of ultrafast camera-based imaging of single fluorescent molecules and live-cell PALM. *BioRxiv* 2021.10.26.465864 (2021) doi:10.1101/2021.10.26.465864.

57. Fujiwara, T. K. *et al.* Focal adhesion membrane is dotted with protein islands and partitioned for molecular hop diffusion. *BioRxiv* 2021.10.26.465868 (2021) doi:10.1101/2021.10.26.465868.

58. Bindels, D. S. *et al.* mScarlet: a bright monomeric red fluorescent protein for cellular imaging. *Nat. Methods* **14**, 53–56 (2017).

59. Maekawa, M. & Fairn, G. D. Complementary probes reveal that phosphatidylserine is required for the proper transbilayer distribution of cholesterol. *J. Cell Sci.* **128**, 1422–1433 (2015).

60. Johnson, B. B. *et al.* Modifications in perfringolysin O domain 4 alter the cholesterol concentration threshold required for binding. *Biochemistry* **51**, 3373–3382 (2012).

61. Ilić, D. *et al.* Extracellular matrix survival signals transduced by focal adhesion kinase suppress p53-mediated apoptosis. *J. Cell Biol.* **143**, 547–560 (1998).

62. Lee, HS., Anekal, P., Lim, C. J., Liu, CC. & Ginsberg, M. H. Two modes of integrin activation form a binary molecular switch in adhesion maturation. *Mol. Biol. Cell* **24**, 1354–1362 (2013).

63. Tsuruta, D. *et al.* Microfilament-dependent movement of the β3 integrin subunit within focal contacts of endothelial cells. *FASEB J.* **16**, 866–868 (2002).

64. Okrut, J., Prakash, S., Wu, Q., Kelly, M. J. S. & Taunton, J. Allosteric N-WASP activation by an inter-SH3 domain linker in Nck. *Proc. Natl Acad. Sci. USA* **112**, E6436–E6445 (2015).

65. Sun, Y., Thapa, N., Hedman, A. C. & Anderson, R. A. Phosphatidylinositol 4,5-bisphosphate: targeted production and signaling. *Bioessays* **35**, 513–522 (2013).

66. Uchida, Y. *et al.* Intracellular phosphatidylserine is essential for retrograde membrane traffic through endosomes. *Proc. Natl Acad. Sci. USA* **108**, 15846–15851 (2011).

67. Diamond, L. E. *et al.* Human CD59 expressed in transgenic mouse hearts inhibits the activation of complement. *Transpl. Immunol.* **3**, 305–312 (1995).

68. Johannessen, C. M. *et al.* COT drives resistance to RAF inhibition through MAP kinase pathway reactivation. *Nature* **468**, 968–972 (2010).

69. Jones, N. P., Peak, J., Brader, S., Eccles, S. A. & Katan, M. PLCγ1 is essential for early events in integrin signalling required for cell motility. *J. Cell Sci.* **118**, 2695–2706 (2005).

70. Ishida, S., Matsu-ura, T., Fukami, K., Michikawa, T. & Mikoshiba, K. Phospholipase C-β1 and β4 contribute to non-genetic cell-to-cell variability in histamine-induced calcium signals in HeLa cells. *PLoS One* **9**, e86410 (2014).

71. Sasaki, A. *et al.* Mammalian Sprouty4 suppresses Ras-independent ERK activation by binding to Raf1. *Nat. Cell Biol.* **5**, 427–432 (2003).

72. Lindberg, F. P., Gresham, H. D., Schwarz, E. & Brown, E. J. Molecular cloning of integrin-associated protein: an immunoglobulin family member with multiple membrane-spanning domains implicated in alpha v beta 3-dependent ligand binding. *J. Cell Biol.* **123**, 485–496 (1993).

73. Nakamura, A. *et al.* Engineering orthogonal, plasma membrane-specific SLIPT systems for multiplexed chemical control of signaling pathways in living single cells. *ACS Chem. Biol.* **15**, 1004–1015 (2020).

74. Fujiwara, T., Ritchie, K., Murakoshi, H., Jacobson, K. & Kusumi, A. Phospholipids undergo hop diffusion in compartmentalized cell membrane. *J. Cell Biol.* **157**, 1071–1082 (2002).

75. Koyama-Honda, I. *et al.* Fluorescence imaging for monitoring the colocalization of two single molecules in living cells. *Biophys. J.* **88**, 2126–2136 (2005).

76. Shibata, A. C. E. *et al.* Archipelago architecture of the focal adhesion: membrane molecules freely enter and exit from the focal adhesion zone. *Cytoskeleton* **69**, 380–392 (2012).

77. Tsunoyama, T. A. *et al.* Super-long single-molecule tracking reveals dynamic-anchorage-induced integrin function. *Nat. Chem. Biol.* **14**, 497–506 (2018).

78. Sahl, S. J., Leutenegger, M., Hilbert, M., Hell, S. W. & Eggeling, C. Fast molecular tracking maps nanoscale dynamics of plasma membrane lipids. *Proc. Natl Acad. Sci. USA* **107**, 6829–6834 (2010).

79. Veatch, S. L. *et al.* Correlation functions quantify super-resolution images and estimate apparent clustering due to over-counting. *PLoS One* **7**, e31457 (2012).

80. Xu, K., Zhong, G. & Zhuang, X. Actin, spectrin, and associated proteins form a periodic cytoskeletal structure in axons. *Science* **339**, 452–456 (2013).

81. Lee, SH., Shin, J. Y., Lee, A. & Bustamante, C. Counting single photoactivatable fluorescent molecules by photoactivated localization microscopy (PALM). *Proc. Natl Acad. Sci. USA* **109**, 17436–17441 (2012).

82. Zitter, E. D. *et al.* Mechanistic investigation of mEos4b reveals a strategy to reduce track interruptions in sptPALM. *Nat. Methods* **16**, 707–710 (2019).

83. Ovesný, M., Křížek, P., Borkovec, J., Švindrych, Z. & Hagen, G. M. ThunderSTORM: a comprehensive ImageJ plug-in for PALM and STORM data analysis and super-resolution imaging. *Bioinformatics* **30**, 2389–2390 (2014).

84. Dundr, M. & Misteli, T. Measuring dynamics of nuclear proteins by photobleaching. *Curr. Protoc. Cell Biol.* **18**, 13.5.1-13.5.18 (2003).

85. Otsu, N. A threshold selection method from gray-level histograms. *IEEE Trans. Syst. Man Cybern.* **9**, 62–66 (1979).

86. Anthis, N. J. & Clore, G. M. Sequence-specific determination of protein and peptide concentrations by absorbance at 205 nm: sequence-specific protein concentration at 205 nm. *Protein Sci.* **22**, 851–858 (2013).

87. Schindelin, J. *et al.* Fiji: an open-source platform for biological-image analysis. *Nat. Methods* **9**, 676–682 (2012).

88. Berg, S. *et al.* ilastik: interactive machine learning for (bio)image analysis. *Nat. Methods* **16**, 1226–1232 (2019).

Acknowledgements

We thank the following PIs for the kind gifts of cell lines: M. Sokabe (Nagoya University) for T24 cells; R. Fässler (Max Planck Institute of Biochemistry) for the talin1/2-dKO MEFs and talin2-KO MEFs; M. C. Beckerle (University of Utah) for the zyxin-KO MEFs; N. Mizushima (University of Tokyo) for the control MEF lines 1-3; R. Kuwahara (OIST) for the control MEF line 4; and V. Horejsi (Institute of Molecular Genetics of the Czech Academy of Sciences) for the hybridoma MEM43/5. We are grateful to the following PIs for the kind gifts of cDNAs encoding the indicated proteins: R. J. Morris (King's College London) for rat Thy1; L. L. Looger (Janelia Research Campus) for mEos2; C. H. Damsky (University of California, San Francisco) for mouse FAK; C. J. Lim (University of California, San Diego) for human RIAM; J. C. Jones (Northwestern University) for human β3 integrin; J. Taunton (University of California, San Francisco) for rat N-WASP; R. A. Anderson (University of Wisconsin) for mouse PIP5KIγ; T. Itoh (Kobe University) for various probes binding to phosphoinositides; T. Taguchi (Tohoku University) for the PS binding probe; P. D. Camilli (Yale University) for CIBN and CRY2-5ptase; M. Tone (Oxford University) for human CD59; W. Hahn and D. Root (Broad Institute of MIT and Harvard) for human PDGFR-β; M. Katan (Cancer Research UK Centre) for rat PLCγ1; K. Mikoshiba (ShanghaiTech University) for mouse PLCβ1; A. Yoshimura (Keio University) for human K-Ras and Raf1; and E. C. Brown (Genentech) for human CD47. We also thank P. Kanchanawong and S. Liu, and M. Kham (National University of Singapore) for technical support for the mouse embryonic stem cell culture, P. Barzaghi and B. Humbel (OIST Imaging Section) for technical support for the FRAP experiments using the Nikon A1R confocal microscope, and all members of the Kusumi laboratory for valuable discussions. This work was supported in part by Japan Society for the Promotion of Science (JSPS) Grants-in-Aid for Scientific Research (Kiban A to A.K. [21H04772], Kiban S to A.K. [16H06386], Kiban B to T.K.F. [16H04775], Kiban C to R.S.K. [17K07333], Wakate B to R.S.K. [26870292], Wakate to T.A.T. [21K15058], and Challenging Exploratory Research to T.K.F. [18K19001]), a Grant-in-Aid for Innovative Areas from the Ministry of Education, Culture, Sports, Science and Technology of the Japanese government (MEXT) to K.G.N.S. (18H04671), a Japan Science and Technology Agency (JST) grant in the program of the Core Research for Evolutional Science and Technology (CREST) in the field of "Biodynamics" to A.K. and that in the field of "Extracellular Fine Particles" to K.G.N.S. (JPMJCR18H2), and a JST grant ACT-X to T.A.T. (JPMJAX211B). WPI-iCeMS of Kyoto University is supported by the World Premiere Research Center Initiative (WPI) of MEXT.

Author contributions

T.A.T. performed large majorities of the single-fluorescent-molecule imaging, biochemistry, and molecular biology experiments and their analyses. T.A.T., T.K.F., and A.K. developed the single-molecule imaging camera system, set up single-molecule imaging stations, and developed the analysis software. C.H. and D.M purified zyxin and VASP and, together with T.A.T., performed LLPS and FRAP experiments. B.T. generated protein probes for cholesterol and sphingomyelin. T.A.T., Y.L.N., K.M.H., R.S.K., T.K.F., K.G.N.S., C.H., D.M., and A.K. participated in discussions throughout the course of this research. T.A.T., T.K.F., K.G.N.S., and A.K. conceived and formulated this project, and evaluated and discussed data. T.A.T. and A.K. wrote the manuscript and all authors participated in its revision.

Competing interest declaration

The authors declare no competing interests.

Additional Information

Supplementary Information is available for this paper.
Correspondence and requests for materials should be addressed to A.K.